JACS
JOURNAL OF THE AMERICAN CHEMICAL SOCIETY

ARTICLE

pubs.acs.org/JACS

Structure, Chemical Composition, And Reactivity Correlations during the In Situ Oxidation of 2-Propanol

Kristof Paredis,[†] Luis K. Ono,[†] Simon Mostafa,[†] Long Li,[‡] Zhongfan Zhang,[‡] Judith C. Yang,[‡,§] Laura Barrio,[∥] Anatoly I. Frenkel,[⊥,*] and Beatriz Roldan Cuenya[†,*]

[†]Department of Physics, University of Central Florida, Orlando, Florida 32816, United States

[‡]Department of Mechanical Engineering and Materials Science, University of Pittsburgh, Pittsburgh, Pennsylvania 15261, United States

[§]Department of Chemical and Petroleum Engineering, University of Pittsburgh, Pittsburgh, Pennsylvania 15261, United States

[∥]Instituto de Catálisis y Petroleoquímica, CSIC, Madrid 28049

[⊥]Department of Physics, Yeshiva University, New York, New York 10016, United States

Supporting Information

ABSTRACT: Unraveling the complex interaction between catalysts and reactants under operando conditions is a key step toward gaining fundamental insight in catalysis. We report the evolution of the structure and chemical composition of size-selected micellar Pt nanoparticles (~1 nm) supported on nanocrystalline γ-Al_2O_3 during the catalytic oxidation of 2-propanol using X-ray absorption fine-structure spectroscopy. Platinum oxides were found to be the active species for the partial oxidation of 2-propanol (<140 °C), while the complete oxidation (>140 °C) is initially catalyzed by oxygen-covered metallic Pt nanoparticles, which were found to regrow a thin surface oxide layer above 200 °C. The intermediate reaction regime, where the partial and complete oxidation pathways coexist, is characterized by the decomposition of the Pt oxide species due to the production of reducing intermediates and the blocking of O_2 adsorption sites on the nanoparticle surface. The high catalytic activity and low onset reaction temperature displayed by our small Pt particles for the oxidation of 2-propanol is attributed to the large amount of edge and corner sites available, which facilitate the formation of reactive surface oxides. Our findings highlight the decisive role of the nanoparticle structure and chemical state in oxidation catalytic reactions.

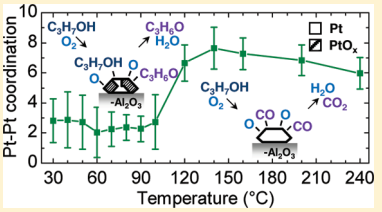

INTRODUCTION

The rational design of the next-generation of catalysts requires detailed knowledge of the correlation between structure, chemical composition, and reactivity. Despite Pt being the most industrially relevant and widely investigated catalyst, its complex interaction with common reactants such as oxygen still provides many challenges to the scientific community.[1] Gaining insight into the nature and structure of the catalytically active Pt species and their interaction with adsorbates under reaction conditions is therefore key in understanding and controlling catalytic activity.[2−11] The downscaling of the catalysts to the nanometer range further complicates the interpretation due to the possible existence of crystallographically and chemically metastable phases, the presence of different surface facets in nanoparticles (NPs) with distinct size and shape, the interaction with the support, and a variety of additional parameters.[1,12−22] Therefore, obtaining unambiguous results on the origin of a particular catalytic performance requires nearly monodispersed NPs in size, shape, and chemical composition.[14]

The present study takes advantage of micellar encapsulation methods for the synthesis of model nanocatalysts with well-defined geometries.[14,23] Such systems are used to address the effect of the NP structure and oxidation state on the catalytic activity and selectivity of Pt NPs supported on γ-Al_2O_3 for the oxidation of 2-propanol. Besides gaining fundamental understanding on structure−reactivity relationships, chemical processes involving the oxidation of alcohols are of importance for the industrial synthesis of fine chemicals as well as for their subsequent removal from the waste streams.[24,25]

Despite intense research efforts, the mechanism behind the oxidation of alcohols over noble metal catalysts is still under debate. Several models have been proposed. The classical dehydrogenation involves two successive dehydrogenation steps of the adsorbed alcohol. The oxygen is merely used to oxidize the released hydrogen in order to vacate metallic sites.[24,26−28] Another suggested pathway is the direct interaction of surface oxygen species with the adsorbed alcohol (or its partially dehydrogenated intermediate).[24,27,29] The third approach also favors the dehydrogenation of the adsorbed alcohol, but is followed by the oxidative removal of the reaction intermediates, rather than the hydrogen.[24,30] These results indicate that the role of oxygen has not yet been uniquely determined. Furthermore, in the case of Pt, the formation of oxidized compounds during oxidation reactions and the resulting influence on the reaction kinetics is still heavily debated. Some studies report catalyst deactivation due to

Received: January 7, 2011
Published: April 06, 2011

oxide formation,[26,27,31−33] while others attribute beneficial catalytic properties to the platinum oxides.[34−40] For instance, the catalytic activity of Pt NPs for the oxidation of carbon monoxide has been attributed to the formation of highly reactive surface oxide phases generated under oxygen-rich reaction conditions.[38,41−43] Clearly, the formation of oxide species plays an important role in oxidation reactions and it is therefore of great importance for the identification of the structure and chemical composition of the catalytically active phase.[44−50]

The method of X-ray absorption fine structure (XAFS) spectroscopy, which allows element-specific structural and chemical analysis under operando conditions, has been used to investigate the catalytic oxidation of 2-propanol. In particular, we have evaluated the stability and reactivity of chemisorbed oxygen species and Pt oxides during the oxidation of 2-propanol over size-selected Pt NPs. Thanks to the well-defined NP morphology and in situ real-time characterization, insight into the detailed mechanisms guiding oxidation reactions will be gained.

EXPERIMENTAL SECTION

(a). Sample Preparation. Dissolving a nonpolar/polar diblock copolymer (polystyrene-block-poly(2-vinylpyridine), PS-P2VP) in toluene results in the formation of inverse micelles which are loaded with a metal precursor (H_2PtCl_6) to create encapsulated NPs. By varying the polymer head length and adjusting the metal salt-polymer head ratio (L), NPs with distinct sizes and shapes can be synthesized.[23] The NPs are deposited on commercial nanocrystalline (powder) γ-Al_2O_3 supports (~40 nm average grain size) by adding the support to the NP polymeric solution. Subsequently, the solvent is evaporated and the polymer removed by a 24 h annealing treatment at 375 °C in an oxygen atmosphere. The latter treatment results in the partial oxidation of the NPs and the formation of core(Pt-metal)-shell(PtO_x) NPs.[23,44] For strongly interacting NP/support systems (e.g., Pt/γ-Al_2O_3), annealing small NP micelles with low metal loadings was found to lead to flat 2D-like NPs.[23] For this study, NPs encapsulated by PS(16000)-P2VP(3500) with a metal/P2VP ratio L of 0.05 were prepared.[14] Our annealing pretreatment in O_2 resulted in carbon and chlorine-free NPs as verified by XPS.[14,23] The Pt weight loading was 1%. For the high-angle annular dark-field scanning transmission electron microscopy (HAADF-STEM) measurements, the Pt/γ-Al_2O_3 powders were dissolved in ethanol, and a drop of this solution was placed onto a Cu grid coated with an ultrathin carbon film (Ted Pella, Inc.) and subsequently dried in air. Information on the NP diameter and average size distribution was obtained by measuring the full width at half-maximum of the HAADF intensity profile across the NPs.

(b). Analysis of the Structure and Chemical Composition (EXAFS, XANES). Extended X-ray absorption fine structure spectroscopy (EXAFS) and near-edge spectroscopy (XANES) measurements were conducted at beamline X18B of the National Synchrotron Light Source (NSLS) at Brookhaven National Laboratory. The catalyst (25 mg) was loaded into a reactor cell compatible with transmission XAFS spectroscopy measurements, and interfaced to a quadrupole mass spectrometer to evaluate the catalytic performance up to 240 °C. Mass flow controllers were used to feed a stream of ~2% propanol and ~20% O_2 balanced with He to a total flow of 25 mL/min. Prior to the reaction, the Pt NPs were reduced for 1 h in H_2 at 260 °C.

After acquisition (three scans were averaged at each temperature), the XAFS data were imported into the ATHENA software and aligned using as reference a simultaneously measured Pt foil. Subsequently, the smooth isolated atom background was removed using the AUTOBK algorithm.[51−53] Theoretical models for the data analysis were calculated for platinum and platinum oxide (based on the crystal structure of $Na_2Pt(OH)_6$) using the FEFF6 code and fitted to the EXAFS spectra with the Artemis package.[54,55] First shell fitting was performed in r-space after Fourier transformation of the k^2-weighted data. The typical r-ranges were 1.3−3.2 Å, whereas the k-ranges were typically 2.5−12 $Å^{-1}$. The best fit value for the passive electron reduction factor was obtained from the Pt foil data, and was fixed to 0.86 for all the nanoparticle analyses. The fit parameters and fit quality results are summarized in Table 2 of the Supporting Information (SI). Additional representative XANES and EXAFS data, together with corresponding fits, can also be found in SI Figures 1−4.

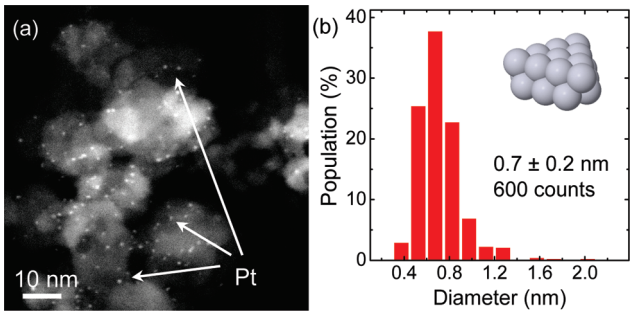

Figure 1. (a) HAADF-STEM micrograph of micellar Pt NPs supported on γ-Al_2O_3 taken after polymer removal and subsequent 2-propanol oxidation. The corresponding diameter histogram is shown in (b).

RESULTS

(a). Structure and Morphology (TEM, EXAFS). Figure 1 shows a HAADF-STEM micrograph of the polymer-free γ-Al_2O_3-supported Pt NPs (a), along with the corresponding diameter histogram (b). The data were acquired after the propanol oxidation reaction. A detailed size analysis revealed a 0.7 ± 0.2 nm average NP diameter and a 0.9 ± 0.3 nm volume-weighted NP diameter. In a previous study by our group, the shape of similarly prepared NPs was resolved via EXAFS, STEM and cluster shape modeling after reduction in H_2, yielding a two-dimensional truncated octahedron as most representative shape.[14,22,23] A similar analysis was carried out here for the NPs under investigation before exposure to the reactants, and an analogous 2D-shape was obtained (see SI for details). A representative image of this shape is presented as inset in Figure 1(b).

We took special care to estimate the degree of structural and morphological homogeneity of nanoparticles within the sample, which is a requirement when EXAFS results are interpreted in terms of an average size and shape of a representative nanoparticle. Although the vast majority of the NPs in this sample were distributed within a narrow range of sizes below 1.3 nm (see Figure 1), a small number of larger Pt particles (with a mean size of ~13 nm) were detected by TEM in some regions of the sample. To evaluate the possible effect of these large particles on the structural model deduced from the analysis of the combined EXAFS and STEM data, as well as on the reaction mechanism, we estimated the overall number density of the large particles by a method described in the SI. Our results demonstrate that the number of small particles significantly exceeds the number of large particles in the sample by a factor of ca. 20 000, that they occupy ~85% of the total Pt volume of the sample, and that their share of the total number of surface atoms, responsible for the reactive behavior of the Pt NPs is ~99%.

EXAFS data acquired at room temperature after NP reduction at 260 °C in H_2 before and after the 2-propanol oxidation reaction

dx.doi.org/10.1021/ja200178f | J. Am. Chem. Soc. 2011, 133, 6728–6735

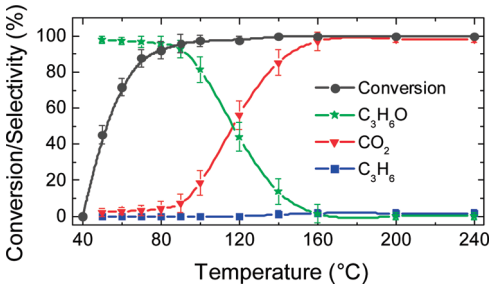

Figure 2. Conversion and selectivity data as a function of temperature for the steady state oxidation of 2-propanol over micellar Pt NPs supported on γ-Al_2O_3.

(see SI Figure 5), revealed the overall structural stability of the NPs in this sample, since similar EXAFS spectra (within experimental noise) were recorded in both instances, indicating the lack of significant NP coarsening and/or structural reconstruction. This result is in agreement with the TEM data shown in Figure 1, since the image was acquired after reactant exposure.

(b). Catalytic Reactivity. Figure 2 summarizes the temperature dependence of the conversion of 2-propanol over our Pt NPs under steady-state reaction conditions. The ~50 °C onset reaction temperature (defined as the 50% conversion temperature) of these 2D-shaped NPs is in accordance with our earlier study[14] and considerably lower than that of 3D NPs of similar TEM diameter (>65 °C, ref 14). This difference is attributed to the larger number of undercoordinated active reaction sites available on the NP surface of the bilayer 2D NPs.[14] Our 2D Pt catalysts reach a 100% conversion of 2-Propanol at 140 °C. The main reaction products observed are acetone, carbon dioxide, and water, as expected from the partial and complete oxidation of 2-propanol:

$$C_3H_7OH + 1/2\ O_2 \rightarrow C_3H_6O + H_2O \quad (1)$$

$$C_3H_7OH + 9/2\ O_2 \rightarrow 3\ CO_2 + 4\ H_2O \quad (2)$$

Figure 2 also displays the product selectivity. Initially, high selectivity (>97%) for acetone (reaction pathway 1) is observed, but with increasing temperature the reaction gradually shifts to the complete oxidation (reaction pathway 2), reaching a CO_2 selectivity of more than 98%. In addition, above 140 °C a small fraction of propene (<2%) is observed, which originates from the dehydration of 2-propanol on the γ-Al_2O_3 support.[56,57]

(c). In Situ Evolution of the Structure and Chemical Composition of Pt NP Catalysts (XANES, EXAFS). Figure 3(a) presents Pt L_3 XANES spectra of micellar Pt NPs on γ-Al_2O_3 during various steady state stages of the reaction. As was mentioned before, the removal of the encapsulating polymeric ligands by the 24 h anneal in O_2 results in core−shell oxidized NPs.[23] Since the L_3 transition probes the empty 5*d* states, oxidation leads to a higher edge intensity (white line), as observed for the partially oxidized as-prepared sample.[58] By comparing the shape of the XANES spectrum of the as-prepared NPs to literature reports on Pt oxide powders (see SI Figure 1), we conclude that PtO_2 is the most likely species present as NP shell.[54,59,60] A considerable decrease in the white line intensity was observed upon reduction in H_2. After the introduction of the reactants (O_2 and 2-propanol), the spectrum recorded at 40 °C

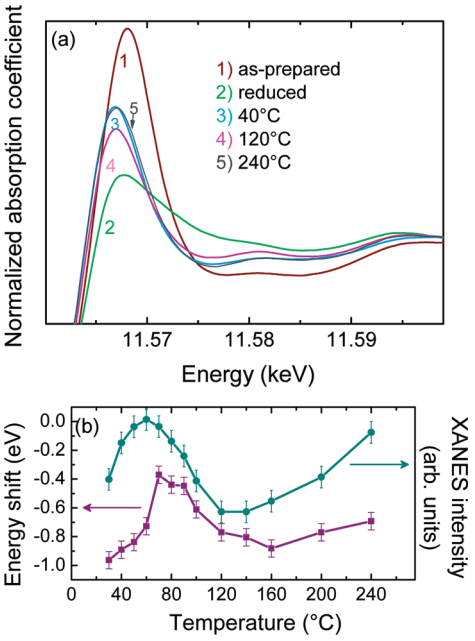

Figure 3. (a) Pt L_3 XANES spectra recorded after polymer removal (in O_2 at 375 °C, as-prepared), after reduction (in H_2 at 260 °C), and during the oxidation of 2-propanol (under 2-propanol and O_2 flow). (b) Integrated XANES intensity (right axis) and absorption peak energy shift relative to the reduced state of the same NPs (left axis) as a function of the reaction temperature.

(i.e., before the onset of the alcohol conversion) shows an increased white line intensity as compared to the fully reduced spectrum, yet still lower than the original oxidic spectrum of the as-prepared samples. This result points to a reduced extent of oxidation. Interestingly, the white line intensity shows a decrease at 120 °C and a subsequent increase at 240 °C, such effects will be described in more detail in the Discussion section.

The detailed evolution of the integrated white line intensity during the reaction is quantitatively summarized in Figure 3(b). Initially a slight increase of the intensity of the absorption peak is observed, coinciding with the onset of alcohol conversion. With increasing temperature, the intensity steadily decreases to reach a minimum at 120−140 °C, at which point the complete oxidation is the dominating reaction pathway, and subsequently increases again with temperature. Since the white line intensity is influenced by NP/adsorbate charge transfer phenomena, more specifically, by the electronegativity of the adsorbates, these variations point to a change in adsorbate composition or coverage during the various stages of the reaction.[33,38,58,61,62] Size effects, charge transfer phenomena between the NPs and the support, are also known to affect the XANES region.[63,64] Since the average NP size was found to remain quasi constant throughout the reaction (see SI Figure 5), and dramatic changes in the NP/support interaction are not likely to occur within this relatively small temperature regime, they are expected to have a minor influence. Therefore, the changes in the XANES data displayed in Figure 3(b) are dominated by NP/adsorbate interactions.[65]

Along with the integrated intensity, Figure 3(b) also presents the energy shift of the maximum of the Pt L_3 adsorption edge relative to the absorption peak of the reduced particles. The shift of the main edge to lower or higher energies is often attributed to the transfer of electronic density to or from the X-ray absorbing

dx.doi.org/10.1021/ja200178f |*J. Am. Chem. Soc.* 2011, 133, 6728–6735

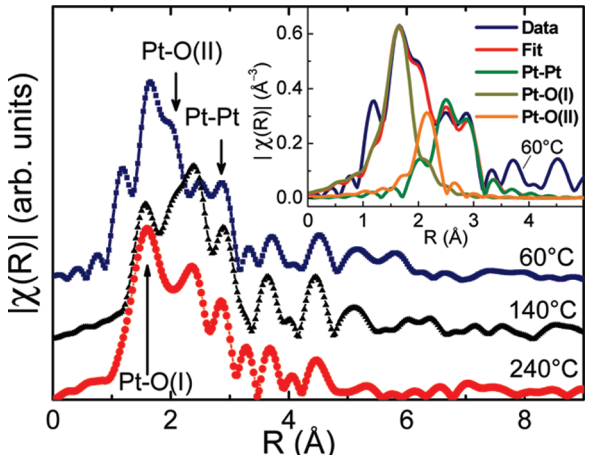

Figure 4. Fourier transformed Pt L_3 edge spectra taken at 60 °C (squares), 140 °C (triangles) and 240 °C (circles) under reactant flow (k^2-weighted, 2.5< k <12 $Å^{-1}$). The spectra are vertically displaced for clarity. The inset shows the magnitude of the data and the fit with the corresponding contributions to the 60 °C spectrum.

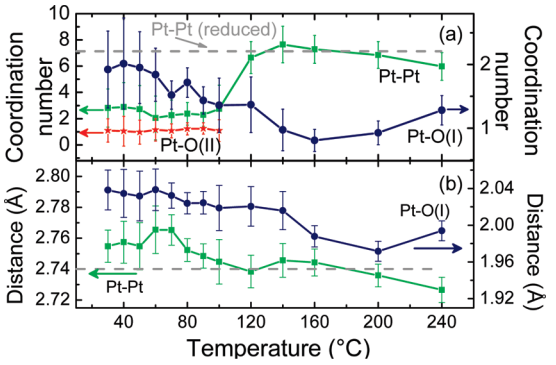

Figure 5. (a) Dependence of the first nearest neighbor coordination number on the reaction temperature during the oxidation of 2-propanol over Pt NPs supported on γ-Al_2O_3: the Pt−Pt, Pt−O(I), and Pt−O(II) contribution for the small 2D NPs obtained from the fitting of in situ EXAFS spectra are shown. The dashed gray line indicates the Pt−Pt coordination number after NP reduction in H_2 and before reactant exposure. (b) Pt−Pt and Pt−O(I) bond distances as a function of temperature. The dashed gray line indicates the Pt−Pt distance after NP reduction in H_2. Note the different *y*-scales in both graphs.

atom, respectively. Its interpretation in nanoscale metal clusters is sometimes complicated by additional factors, namely, the increase in the Fermi level energy as well as the increase in the electronic screening, since both effects lead to blue and red shifts of the X-ray absorption edge, respectively.[66] Therefore, the shift of the absorption edge measured cannot be used by itself to determine the direction of charge transfer. As demonstrated in Figure 3(b), the energy shift follows a similar trend to the integrated intensity; an initial increase with a maximum at 70 °C, followed by a slow decrease up to 160 °C, and a slight increase at higher temperature. Since the two effects, the change in the white line intensity and the shift of the absorption edge, correlate with each other in terms of the direction of the charge transfer, they can be interpreted self-consistently in terms of the same origin.

Figure 4 shows Fourier transformed k^2-weighted Pt L_3 EXAFS data acquired in situ at different temperatures (60 °C, 140 °C, and 240 °C) under reaction conditions, that is, under a simultaneous flow of 2-propanol and O_2. These spectra were fitted with various contributions resulting from Pt atoms in different chemical environments: (1) Pt−O(I) due to a chemisorbed O layer or the presence of an oxide, (2) Pt−O(II) due to the presence of adsorbed 2-propanol on Pt, and (3) Pt−Pt for the metallic Pt component. The different fitting contributions are illustrated in the inset of Figure 4 for the 60 °C spectrum and allow the determination of the respective first nearest neighbor coordination numbers (N_{Pt-Pt}, $N_{Pt-O(I)}$, $N_{Pt-O(II)}$) and distances (d_{Pt-Pt}, $d_{Pt-O(I)}$, and $d_{Pt-O(II)}$). The fits of the 140 and 240 °C data can be found in SI Figure 3. The coordination numbers and the corresponding distances are presented as a function of temperature in Figure 5(a) and (b), respectively. The distance of the Pt−O(II) component, 2.53 ± 0.05 Å, was found to be nearly constant in the fits and is therefore not shown in Figure 5(b). The horizontal dashed lines refer to the coordination number and distance after NP reduction in H_2 (spectrum taken at room temperature), which was the starting point before exposure to the reactants.

The fitting procedure yields a Pt−Pt coordination N_{Pt-Pt} of 7.1 ± 0.5, with a Pt−Pt distance of 2.74 ± 0.01 Å for the reduced NPs measured in H_2. Upon initial reactant exposure (O_2 and 2-propanol) and in the low temperature reaction regime (<100 °C), the Pt−Pt coordination number significantly decreases, while the average Pt−Pt bond length slightly increases (2.76 ± 0.02 Å). Furthermore, two additional Pt−O contributions are identified. First, a short distance Pt−O(I) pair typical of platinum oxide or chemisorbed oxygen is found at 2.03 ± 0.01 Å. Although the presence of chemisorbed oxygen cannot be excluded, the accompanying decrease of the Pt−Pt contribution clearly points to the formation and stabilization of a surface oxide. This conclusion is based on the property of EXAFS coordination numbers to be related not only to the number of nearest neighboring bonds, but also to the total number of absorbing atoms. Thus, if two phases are present in the sample, one metallic with Pt−Pt bonds, and the other oxide without Pt−Pt bonds, the Pt−Pt coordination number measured in that sample will decrease, as is observed in our case. However, since various Pt oxides (PtO, Pt_3O_4, PtO_2) exhibit similar Pt−O distances and coexistence of different phases might occur, the EXAFS data cannot be used to uniquely assign this contribution to a specific oxide species.[35,67] However, it is clear that the stable PtO_2 compounds initially present on the as-prepared samples (annealed in O_2 for 24 h) are removed by the in situ annealing treatment in H_2 prior to the reaction, since the PtO_2 characteristic features do not reappear after exposure to 2-propanol and oxygen (see SI Figure 1). Second, a long distance Pt−O contribution, Pt−O(II), is observed at 2.53 ± 0.05 Å, which agrees well with the values previously reported for alcohols chemisorbed on Pt, in particular, for 2-propanol on Pt(111).[68−71]

The appearance of the Pt−O(I) contribution is an evidence of the partially oxidized state of the NPs in this temperature regime (<120 °C), which is in agreement with our XANES results. The Pt−O(II) contribution demonstrates the direct adsorption of 2-propanol on Pt, indicating that not all available sites are occupied by oxygen. Despite the oxidation, the EXAFS data still clearly show a Pt−Pt contribution from a metallic phase (see r-range of 2.2 to 3 Å in Figure 4), implying the presence of a metallic NP core. The XANES spectra of our Pt NPs acquired at room temperature after a prolonged annealing treatment in O_2 (24 h) and those measured after in situ reduction and subsequent exposure to the reactants (O_2 + 2-propanol) can be found in SI Figure 6. The strong decrease in the white line intensity in the

dx.doi.org/10.1021/ja200178f |*J. Am. Chem. Soc.* 2011, 133, 6728–6735

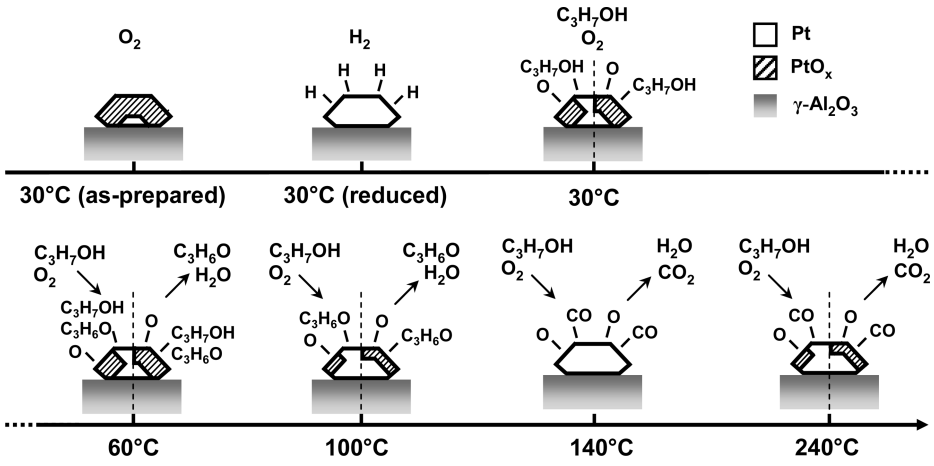

Figure 6. Schematic representation of the catalyst structure in the as-prepared state, after reduction, and during various stages of the reaction. Reactants and products are indicated above the illustrations. Possible alternative mechanisms involving a homogeneous PtOx shell (right) and a 2-phase catalyst composed by PtO_x patches coexisting with metallic Pt regions (left) are separated by the dashed lines.

sample exposed to the reactants as compared to that acquired before NP reduction demonstrates that our NPs are only partially oxidized under reaction conditions.

At reaction temperatures above 120 °C, the Pt−Pt contribution becomes dominant again and the corresponding coordination number returns to the value obtained for the reduced NPs ($N_{Pt-Pt} \approx 7.2$). This result indicates the decomposition of the platinum oxide species and the return of the NPs to the metallic state. The disappearance of the oxide is also reflected in a decrease of the short Pt−O(I) coordination number (from ∼2 to ∼1). However, a minor Pt−O(I) content still remains and together with the metallic state of the particle, this suggests the presence of chemisorbed oxygen on the NP surface. The presence of O on the Pt surface is also reflected by the larger intensity of the XANES white line measured at 120 °C as compared to that of the reduced NPs, Figure 3(a). Interestingly, the Pt−O(II) contribution vanishes above 100 °C, when 100% conversion of 2-propanol is achieved. Parallel to the intensity increase in XANES at temperatures above 200 °C, we also observe a small decrease in Pt−Pt coordination and corresponding increase in Pt−O(I) coordination.

■ DISCUSSION

Although the overall structural stability of our Pt nanocatalysts was evidenced via EXAFS and TEM (NP diameter), small changes in the NP shape during the reaction (e.g., rounding of corners) cannot be ruled out, since they could fall within the error margins of the coordination numbers obtained at different stages of the reaction. In fact, nanoparticle rounding has been observed in environmental TEM studies of Au and Pt NPs under oxygen.[72−75] A complete 2D to 3D shape transformation should however not have taken place in our sample, since such structural transformation would give rise to a clear increase in the coordination numbers, which was not observed here. It should be considered that the NP/support interface might also play a key role in the stabilization of the flat and small (<1 nm) NPs initially available on our sample (after H_2 reduction). In addition, the possible mobility of our NPs in the course of the reaction has not been considered. This assumption is based on the fact that our NPs were pretreated in O_2 (an environment which should in principle facilitate NP mobility) for extended periods of time at higher temperatures (375 °C) than the maximum reaction temperature (240 °C). Therefore, if NP mobility (and possibly coarsening) were born to occur, they would likely have taken place during our 24 h pretreatment in O_2.

Our in situ EXAFS and mass spectrometry data revealed the enhanced activity (low onset reaction temperature) and temperature-dependent selectivity of our micellar Pt NPs for the partial and total oxidation of 2-propanol. In addition, insight into the evolution of the oxidation state of the active nanocatalysts under different reaction conditions could be extracted.

Figure 6 schematically displays the proposed reaction mechanism. As demonstrated by the XANES and EXAFS data, the initially reduced metallic particles immediately partially oxidize upon exposure to the reactant flow (O_2 and 2-propanol) at room temperature. This effect is evidenced by the decrease in the number of Pt−Pt bonds and the concomitant increase in the Pt−O(I) bonding. The decrease of the Pt−Pt coordination could also be due to an adsorbate-induced change in the NP shape, with flatter NPs giving rise to lower coordination numbers. However, a shape change alone cannot cause such a large reduction in Pt−Pt coordination numbers as observed here. Moreover, such effect should also be ruled out here, since the change in the first nearest neighbor coordination number is observed upon reactant exposure, and O_2 is known to cause NP rounding.[72,73] The latter effect should give rise to an increase in Pt−Pt coordination, contrary to the present observation.[76] The presence of chemisorbed oxygen in combination with the oxide cannot be excluded. However, the XANES spectra in Figure 3(a) only show the partial oxidation of the NPs, and Pt−Pt bonding is still observed for both catalysts via EXAFS, reflecting the presence of a metallic NP core. EXAFS also reveals the presence of adsorbed 2-propanol on the NP surface, which indicates that not all Pt sites at the surface are occupied by oxygen. With the onset of 2-propanol conversion (between 40 and 50 °C), the intensity of the XANES white line increases slightly, Figure 3(b), which can be attributed to oxygen atoms occupying surface sites that become available after the desorption of 2-propanol as acetone. Here, 2-propanol and oxygen are not competing for active sites, as varying the O_2 to propanol ratio between 3 and 205 was not found to influence the measured conversion (see SI Figure 7).

dx.doi.org/10.1021/ja200178f |J. Am. Chem. Soc. 2011, 133, 6728–6735

Consequently, based on the evolution of the XANES white line intensity in the temperature regime where the partial oxidation of 2-propanol to acetone takes place and on the corresponding EXAFS data, we can conclude that PtO_x compounds are the catalytically active phase. The large density of step, edge and corner sites in our small 2D (flat) Pt NPs is likely to facilitate the dissociation of O_2 and the subsequent formation of surface oxides for high oxygen coverages. The improved reactivity of metal surfaces with either chemisorbed oxygen or surface oxides has been previously reported.[48] For example, Wang et al.[37] observed that one-dimensional PtO_2 stripes formed at Pt steps react more easily with CO than chemisorbed O on Pt. Although PtO_2 was shown to be the preferential oxide formed on 1 nm sized nanoparticles supported on γ-Al_2O_3, oxide structures with intermediate stoichiometry such as Pt_3O_4 and PtO are also reported to be thermodynamically stable showing enhanced chemical reactivity for CO oxidation and methanol decomposition, respectively.[21,35,44,71,77] Alayon et al.[38] also observed the higher activity of defective Pt oxide species on partially oxidized Pt/Al_2O_3 catalysts for the oxidation of CO as compared to metallic Pt. In the former study, dynamic changes in the structure of the catalysts were observed, with different contents of PtO_x species present under distinct reaction conditions. Furthermore, Smith and co-workers observed that oxygen strongly bonded to kink sites on a Pt surface facilitated dehydrogenation reactions.[78] Since the dehydrogenation is the key step in the partial oxidation of 2-propanol, we believe that the high density of low coordinated sites available on our small 2D-shaped particles and their unique interaction with oxygen are the key features responsible for the catalytic activity of our micellar Pt NPs.

However, even though based on our EXAFS and XANES data it is observed that the catalysts active for the selective partial oxidation of 2-propanol are Pt NPs with a metallic core and an oxide shell. The specific structure of this oxide (PtO, PtO_2 or other PtO_x) cannot be concluded. Since EXAFS does not provide information on the uniformity of the oxide shell, we cannot exclude the presence of metallic Pt at the NP's surface. Therefore, in addition to a homogeneous oxide layer, a nonuniform PtO_x layer is also proposed in Figure 6 (left side of the dashed lines). Interestingly, a decrease in the degree of NP oxidation is not observed during the selective partial oxidation of Propanol (50−70 °C), suggesting a Mars-van Krevelen process, where the oxygen in the surface oxide lattice, which is consumed by hydrogen released in the dehydrogenation of the 2-propanol, is subsequently replenished by dissociated molecular oxygen from the gas phase. Again, the specific NP structure (small size and 2D shape) is here held responsible for its enhanced reactivity with O_2 at relatively low temperatures.

Above 70 °C, a decrease of the XANES intensity, Figure 3(b), along with a decrease in Pt−O coordination, Figure 5(a), is observed. These changes reflect the partial decomposition of the surface oxide. Interestingly, the onset of the Pt oxide decomposition runs parallel to the decrease in the reaction selectivity for acetone. The disappearance of the PtO_x species and return to the metallic state observed by EXAFS at 120 °C, Figure 5(a), coincides with the minimum in the XANES white line intensity, and with the transition from partial to selective complete oxidation. Our data suggest that the activation of the C−C bond (scission) and the subsequent presence of intermediate carbonaceous compounds, such as CO, on the NP surface are responsible for the reduction of the NPs.[33] In fact, the metallic state is reinstated at the temperature where the complete oxidation pathway is preferred. Since PtO_x species are generally stable up to 230 °C in vacuum, these results illustrate that the decomposition of PtO_x is governed by the reaction process, and not by the increasing temperature.[13,60] In summary, the active catalysts for the complete oxidation of 2-propanol are metallic Pt NPs with chemisorbed oxygen adsorbed on their surfaces coexisting with carbonaceous intermediates.

Upon increasing the reaction temperature to 240 °C, the increase in the XANES white line and the Pt−O(I) coordination number were observed. These trends might be attributed to a faster and increased desorption of carbonaceous species from the NP surface, leading to a smaller effective coverage. As a result, more surface sites become available for the dissociation of oxygen and subsequent Pt oxide formation. However, the catalytic activity did not decrease upon the formation of this thin oxide layer, as can be seen in Figure 2. Consequently, in this high temperature regime of the complete oxidation, the active catalysts consist of Pt NPs with a very thin surface oxide layer, likely inhomogeneous in nature with exposed metallic Pt species.

No decrease in the catalytic activity of the Pt NPs was observed under our experimental conditions (O_2-rich flow) during an extended period of time (26 h), indicating that carbon monoxide intermediates are effectively oxidized to CO_2 in the temperature regime corresponding to the total oxidation of propanol. As a result, our small 2D-shaped NPs are not only good catalysts in terms of their low onset reaction temperature, but also with respect to their resistance to poisoning.

Summarizing, our in situ investigation of the structure and chemical composition of nanosized Pt catalysts at work (operando conditions) provides valuable insight on the fundamental mechanisms that govern the catalytic chemistry of oxidation reactions. In particular, it highlights the important role played by surface oxides and chemisorbed oxygen species.

CONCLUSIONS

The evolution of the structure and chemical composition of small two-dimensional Pt NPs supported on γ-Al_2O_3 has been followed in situ during the oxidation of 2-propanol. It is shown that the catalysts undergo significant chemical and structural changes in the course of the reaction. Platinum oxide species were found to be present on the NP surface during the partial oxidation of Propanol to acetone, and suggested to play an active role in the reactivity observed. Due to the large amount of step, edge and corner sites available on our small NPs, the dissociation of O_2 and subsequent formation of surface oxides appears to be favorable, resulting in a low reaction onset temperature (~50 °C). In the complete oxidation regime, the active catalysts are initially metallic NPs with chemisorbed oxygen species on their surface. However, with increasing temperature within the complete oxidation reaction regime, catalyst reoxidation was observed. Such effect might be assigned to a higher availability of reactive sites (step/kink/corner atoms) able to dissociate O_2 upon desorption of intermediate passivating carbonaceous species. The decomposition of PtO_x in the intermediate reaction regime, where partial and total oxidation processes coexist, is attributed to the reducing effect of intermediate carbonaceous species available at the onset of the complete oxidation, as well as to the competition of CO and O_2 for adsorption sites on the NP surface.

Altogether, our research provides valuable insight into the mechanisms underlying the oxidation of 2-propanol over Pt NPs,

featuring marked structure−reactivity correlations, and emphasizing the decisive role played by the NP structure (size and shape) on the formation and stabilization of surface oxides, which have been shown to be directly involved in the present catalytic oxidation process.

■ ASSOCIATED CONTENT

Supporting Information. (i) A description of the method employed to determine the average NP shape as well as to estimate the degree of structural and morphological homogeneity of the NPs, (ii) additional details on the fit parameters and results extracted from EXAFS modeling, (iii) XAFS spectra of the NP sample during different stages of the 2-propanol oxidation together with reference data from bulk metallic Pt and PtO_2, (iv) representative EXAFS data of the NP sample under different reaction conditions in k-space and r-space (including fits), (v) data of the conversion of 2-propanol as a function of the O_2 to 2-propanol ratio. This material is available free of charge via the Internet at http://pubs.acs.org.

■ AUTHOR INFORMATION

Corresponding Author
roldan@physics.ucf.edu; anatoly.frenkel@yu.edu

■ ACKNOWLEDGMENT

We are grateful to Dr. J. R. Croy, E. Zhou, and C. Frye (UCF) for assistance in sample preparation, to Dr. Relja Vasic (BNL) for his help during some of the XAFS measurements, and to F. Behafarid for NP shape modeling. Reactivity studies were supported by DE-FG02-08ER15995. Electron microscopy and synchrotron studies were funded by DOE BES (DE-FG02-03ER15476, DE-FG02-05ER15688). NFCF at the University of Pittsburgh is acknowledged for the use of JEM 2100F. Use of NSLS was supported by DOE (DE-AC02-98CH10866). B.R.C. would like to thank Prof. H. J. Freund for kindly hosting her sabbatical research stay at the Fritz-Haber-Institute (Berlin, Germany), where part of this manuscript was written.

■ REFERENCES

(1) Roldan Cuenya, B. *Thin Solid Films* **2010**, *518*, 3127.
(2) Bultel, L.; Roux, C.; Siebert, E.; Vernoux, P.; Gaillard, F. *Solid State Ionics* **2004**, *166*, 183.
(3) Vernoux, P.; Gaillard, F.; Bultel, L.; Siebert, E.; Primet, M. *J. Catal.* **2002**, *208*, 412.
(4) Vayenas, C. G.; Bebelis, S.; Ladas, S. *Nature* **1990**, *343*, 625.
(5) Singh, J.; Alayon, E.; Tromp, M.; Safonova, O.; Glatzel, P.; Nachtegaal, M.; Frahm, R.; van Bokhoven, J. *Angew. Chem.* **2008**, *120*, 9400.
(6) Singh, J.; Nachtegaal, M.; Alayon, E. M. C.; Stotzel, J.; van Bokhoven, J. A. *Chem. Cat. Chem.* **2010**, *2*, 653.
(7) Singh, J.; van Bokhoven, J. A. *Catal. Today* **2010**, *155*, 199.
(8) Xu, Y.; Shelton, W. A.; Schneider, W. F. *J. Phys. Chem. A* **2006**, *110*, 5839.
(9) Ellinger, C.; Stierle, A.; Robinson, I. K.; Nefedov, A.; Dosch, H. *J. Phys.: Condens. Matter* **2008**, *20*, 184013.
(10) Tao, F.; Salmeron, M. *Science* **2011**, *331*, 171.
(11) Pozdnyakova, O.; Teschner, D.; Wootsch, A.; Krohnert, J.; Steinhauer, B.; Sauer, H.; Toth, L.; Jentoft, F. C.; Knop-Gericke, A.; Paal, Z.; Schlogl, R. *J. Catal.* **2006**, *237*, 1.
(12) Narayanan, R.; El-Sayed, M. A. *Nano Lett.* **2004**, *4*, 1343.
(13) Ono, L. K.; Yuan, B.; Heinrich, H.; Roldan Cuenya, B. *J. Phys. Chem. C* **2010**, *114*, 22119.
(14) Mostafa, S.; Behafarid, F.; Croy, J. R.; Ono, L. K.; Li, L.; Yang, J.; Frenkel, A. I.; Roldan Cuenya, B. *J. Am. Chem. Soc.* **2010**, *132*, 15714.
(15) Karim, A. M.; Prasad, V.; Mpourmpakis, G.; Lonergan, W. W.; Frenkel, A. I.; Chen, J. G.; Vlachos, D. G. *J. Am. Chem. Soc.* **2009**, *131*, 12230.
(16) Croy, J. R.; Mostafa, S.; Liu, J.; Sohn, Y.; Heinrich, H.; Roldan Cuenya, B. *Catal. Lett.* **2007**, *119*, 209.
(17) Narayanan, R.; El-Sayed, M. A. *J. Phys. Chem. B* **2005**, *109*, 12663.
(18) Oudenhuijzen, M. K.; van Bokhoven, J. A.; Ramaker, D. E.; Koningsberger, D. C. *J. Phys. Chem. B* **2004**, *108*, 20247.
(19) Ono, L. K.; Roldan Cuenya, B. *Catal. Lett.* **2007**, *113*, 86.
(20) Croy, J. R.; Mostafa, S.; Liu, J.; Sohn, Y.-h.; Roldan Cuenya, B. *Catal. Lett.* **2007**, *118*, 1.
(21) Croy, J. R.; Mostafa, S.; Hickman, L.; Heinrich, H.; Roldan Cuenya, B. *Appl. Catal., A* **2008**, *350*, 207.
(22) Mostafa, S.; Croy, J. R.; Heinrich, H.; Roldan Cuenya, B. *Appl. Catal., A* **2009**, *366*, 353.
(23) Roldan Cuenya, B.; Croy, J. R.; Mostafa, S.; Behafarid, F.; Li, L.; Zhang, Z.; Yang, J. C.; Wang, Q.; Frenkel, A. I. *J. Am. Chem. Soc.* **2010**, *132*, 8747.
(24) Mallat, T.; Baiker, A. *Chem. Rev.* **2004**, *104*, 3037.
(25) Derwent, R. G.; Pearson, J. K. *Environ. Technol.* **1997**, *18*, 1029.
(26) Markusse, A. P.; Kuster, B. F. M.; Koningsberger, D. C.; Marin, G. B. *Catal. Lett.* **1998**, *55*, 141.
(27) Nicoletti, J. W.; Whitesides, G. M. *J. Phys. Chem.* **1989**, *93*, 759.
(28) Schauermann, S.; Hoffmann, J.; Johanek, V.; Hartmann, J.; Libuda, J. *Phys. Chem. Chem. Phys.* **2002**, *4*, 3909.
(29) Augustine, R. L.; Doyle, L. K. *J. Catal.* **1993**, *141*, 58.
(30) Keresszegi, C.; Bürgi, T.; Mallat, T.; Baiker, A. *J. Catal.* **2002**, *211*, 244.
(31) Hartmann, N.; Imbihl, R.; Vogel, W. *Catal. Lett.* **1994**, *28*, 373.
(32) Olsson, L.; Fridell, E. *J. Catal.* **2002**, *210*, 340.
(33) Carlsson, P.-A.; Österlund, L.; Thormählen, P.; Palmqvist, A.; Fridell, E.; Jansson, J.; Skoglundh, M. *J. Catal.* **2004**, *226*, 422.
(34) Dam, V. A. T.; de Bruijn, F. A. *J. Electrochem. Soc.* **2007**, *154*, B494.
(35) Seriani, N.; Jin, Z.; Pompe, W.; Ciacchi, L. C. *Phys. Rev. B* **2007**, *76*, 155421.
(36) Chen, M. S.; Cai, Y.; Yan, Z.; Gath, K. K.; Axnanda, S.; Goodman, D. W. *Surf. Sci.* **2007**, *601*, 5326.
(37) Wang, J. G.; Li, W. X.; Borg, M.; Gustafson, J.; Mikkelsen, A. Pedersen, T. M.; Lundgren, E.; Weissenrieder, J.; Klikovits, J.; Schmid, M.; Hammer, B.; Andersen, J. N. *Phys. Rev. Lett.* **2005**, *95*, 256102.
(38) Alayon, E. M. C.; Singh, J.; Nachtegaal, M.; Harfouche, M.; van Bokhoven, J. A. *J. Catal.* **2009**, *263*, 228.
(39) Andras, S.; Michael, A. H.; Yates, J. T., Jr. *J. Chem. Phys.* **1992**, *96*, 6191.
(40) John, L. G.; Edward, B. K. *J. Chem. Phys.* **1983**, *78*, 963.
(41) Ackermann, M. D.; Pedersen, T. M.; Hendriksen, B. L. M.; Robach, O.; Bobaru, S. C.; Popa, I.; Quiros, C.; Kim, H.; Hammer, B.; Ferrer, S.; Frenken, J. W. M. *Phys. Rev. Lett.* **2002**, *89*, 046101.
(42) Mallens, E. P. J.; Hoebink, J. H. B. J.; Marin, G. B. *Catal. Lett.* **1995**, *33*, 291.
(43) Ackermann, M. D.; Pedersen, T. M.; Hendriksen, B. L. M.; Robach, O.; Bobaru, S. C.; Popa, I.; Quiros, C.; Kim, H.; Hammer, B.; Ferrer, S.; Frenken, J. W. M. *Phys. Rev. Lett.* **2005**, *95*, 255505.
(44) Croy, J. R.; Mostafa, S.; Heinrich, H.; Roldan Cuenya, B. *Catal. Lett.* **2009**, *131*, 21.
(45) Kulkarni, D.; Wachs, I. E. *Appl. Catal., A* **2002**, *237*, 121.
(46) Hawkins, J. M.; Weaver, J. F.; Asthagiri, A. *Phys. Rev. B* **2009**, *79*, 125434.
(47) Gu, Z.; Balbuena, P. B. *J. Phys. Chem. C* **2007**, *111*, 9877.
(48) Hendriksen, B. L. M.; Ackermann, M. D.; van Rijn, R.; Stoltz, D.; Popa, I.; Balmes, O.; Resta, A.; Wermeille, D.; Felici, R.; Ferrer, S.; FrenkenJoost, W. M. *Nat Chem.* **2010**, *2*, 730.

(49) Mainardi, D. S.; Calvo, S. R.; Jansen, A. P. J.; Lukkien, J. J.; Balbuena, P. B. *Chem. Phys. Lett.* **2003**, *382*, 553.
(50) Gu, Z.; Balbuena, P. B. *J. Phys. Chem. C* **2007**, *111*, 17388.
(51) Ravel, B.; Newville, M. *J. Synchrotron Rad.* **2005**, *12*, 537.
(52) Newville, M. *J. Synchrotron Rad.* **2001**, *8*, 322.
(53) Newville, M.; Livins, P.; Yacoby, Y.; Rehr, J. J.; Stern, E. A. *Phys. Rev. B* **1993**, *47*, 14126.
(54) Setthapun, W.; Williams, W. D.; Kim, S. M.; Feng, H.; Elam, J. W.; Rabuffetti, F. A.; Poeppelmeier, K. R.; Stair, P. C.; Stach, E. A.; Ribeiro, F. H.; Miller, J. T.; Marshall, C. L. *J. Phys. Chem. C* **2010**, *114*, 9758.
(55) Zabinsky, S. I.; Rehr, J. J.; Ankudinov, A.; Albers, R. C.; Eller, M. J. *Phys. Rev. B* **1995**, *52*, 2995.
(56) Zhang, J. H.; Zhou, X. L.; Wang, J. A. *J. Mol. Catal. A* **2006**, *247*, 222.
(57) Burgos, N.; Paulis, M.; Mirari Antxustegi, M.; Montes, M. *Appl. Catal., B* **2002**, *38*, 251.
(58) Yoshida, H.; Nonoyama, S.; Yazawa, Y.; Hattori, T. *Phys. Scr.* **2005**, *2005*, 813.
(59) Christensen, S. T.; Elam, J. W.; Rabuffetti, F. A.; Ma, Q.; Weigand, S. J.; Lee, B.; Seifert, S.; Stair, P. C.; Poeppelmeier, K. R.; Hersam, M. C.; Bedzyk, M. J. *Small* **2009**, *5*, 750.
(60) Kolobov, A. V.; Wilhelm, F.; Rogalev, A.; Shima, T.; Tominaga, J. *Appl. Phys. Lett.* **2005**, *86*, 121909.
(61) Guo, N.; Fingland, B. R.; Williams, W. D.; Kispersky, V. F.; Jelic, J.; Delgass, W. N.; Ribeiro, F. H.; Meyer, R. J.; Miller, J. T. *Phys. Chem. Chem. Phys.* **2010**, *12*, 5678.
(62) Ramaker, D. E.; Koningsberger, D. C. *Phys. Chem. Chem. Phys.* **2010**, *12*, 5514.
(63) Ramaker, D. E.; van Dorssen, G. E.; Mojet, B. L.; Koningsberger, D. C. *Top. Catal.* **2000**, *10*, 157.
(64) Boyanov, B. I.; Morrison, T. I. *J. Phys. Chem.* **1996**, *100*, 16318.
(65) Safonova, O. V.; Tromp, M.; van Bokhoven, J. A.; de Groot, F. M. F.; Evans, J.; Glatzel, P. *J. Phys. Chem. B* **2006**, *110*, 16162.
(66) Sanchez, S. I.; Menard, L. D.; Bram, A.; Kang, J. H.; Small, M. W.; Nuzzo, R. G.; Frenkel, A. I. *J. Am. Chem. Soc.* **2009**, *131*, 7040.
(67) Jacob, T.; Muller, R. P.; Goddard, W. A. *J. Phys. Chem. B* **2003**, *107*, 9465.
(68) Alcala, R.; Greeley, J.; Mavrikakis, M.; Dumesic, J. A. *J. Chem. Phys.* **2002**, *116*, 8973.
(69) Tarmyshov, K. B.; Muller-Plathe, F. *J. Chem. Phys.* **2007**, *126*, 074702.
(70) Greeley, J.; Mavrikakis, M. *J. Am. Chem. Soc.* **2002**, *124*, 7193.
(71) Seriani, N.; Pompe, W.; Ciacchi, L. C. *J. Phys. Chem. B* **2006**, *110*, 14860.
(72) Giorgio, S.; Cabie, M.; Henry, C. R. *Gold Bull.* **2008**, *41*, 167.
(73) Giorgio, S.; Sao Joao, S.; Nitsche, S.; Chaudenson, D.; Sitja, G.; Henry, C. R. *Ultramicroscopy* **2006**, *106*, 503.
(74) Kishita, K.; Sakai, H.; Tanaka, H.; Saka, H.; Kuroda, K.; Sakamoto, M.; Watabe, A.; Kamino, T. *J. Electron Microsc.* **2009**, *58*, 331.
(75) Ramachandran, A. S.; Anderson, S. L.; Datye, A. K. *Ultramicroscopy* **1993**, *51*, 282.
(76) Cabié, M.; Giorgio, S.; Henry, C. R.; Axet, M. R.; Philippot, K.; Chaudret, B. *J. Phys. Chem. C* **2010**, *114*, 2160.
(77) Wang, C.-B.; Lin, H.-K.; Hsu, S.-N.; Huang, T.-H.; Chiu, H.-C. *J. Mol. Catal. A* **2002**, *188*, 201.
(78) Smith, C. E.; Biberian, J. P.; Somorjai, G. A. *J. Catal.* **1979**, *57*, 426.